J. Geomag. Geoelectr., **49**, 827–842, 1997

Two-Dimensional Inversion of Papua New Guinea Data Using 'Least-Blocked' Models

A. K. AGARWAL and J. T. WEAVER

Department of Physics and Astronomy and School of Earth and Ocean Sciences, University of Victoria, Victoria, B.C., V8W 3P6, Canada

(Received February 13, 1995; Revised December 29, 1995; Accepted February 2, 1996)

Magnetotelluric data obtained from a region of Papua New Guinea have been inverted with the aid of a two-dimensional scheme in which the simplest 'least-blocked' model compatible with the data is sought. The average strike direction for the entire region and for all periods is estimated to be approximately N60W. In the rotated frame skew is small everywhere, but ellipticity values remain quite large at some sites, which raises some uncertainty about the assumption of two-dimensionality. Since the data also indicate the presence of local galvanic distortion, a static shift correction has been applied; both the original (rotated) data and the static-shift corrected data have been used to generate 'least-blocked' models. The final models for the two data sets are found to resemble each other quite closely. Both reveal a descending conductive layer beneath a resistive limestone cover of thickness 0.6–0.8 km on southwestern side of the profile increasing to around 2.1–2.4 km on the northeastern side. The one notable difference is that the descending conductive layer divides into two parts separated by a resistive limestone layer in the model obtained from static-shift corrected data, but not in the other.

1. Introduction

The various inversion schemes that are available for inverting two-dimensional magnetotelluric (MT) data have been summarized and discussed by Jones (1993) in his introduction to the COPROD2 exercise. Many of the more popular ones, such as Occam (deGroot-Hedlin and Constable, 1990), Rapid Relaxation Inverse (Smith and Booker, 1991) or Approximate Inverse Mapping (Oldenburg and Ellis, 1991), are based on an over-parameterization of the model followed by minimization of a regularized functional in which the misfit is combined with a stabilizing functional. This functional is usually one requiring that the smoothest best fitting model be sought, with the trade-off between smoothness and fit determined by the assigned value of a regularizing parameter. The 'least-blocked' method employed here is a completely different approach. The model is under-parameterized, leading, unlike the other methods, to an over-determined system of equations in the unknown model parameters. A maximum likelihood estimation of these parameters is conducted by minimizing a misfit of the response function to the measured data. The strategy employed in the method has been briefly described in connection with its application to some synthetic models (Agarwal *et al.*, 1993), to the COPROD2 data (Agarwal and Weaver, 1993), and to data from southern British Columbia (Marquis *et al.*, 1995). It involves the automatic generation of a series of optimized models, based on starting models with successively $3, 4, 5, \ldots$ columns, which stops when the inclusion of an extra column is no longer justified by an improvement of the response fit.

The response of a two-dimensional model is characterized by four real measurements (two for each polarization of the field) such as the real and imaginary parts of the TE and TM complex impedances, or the TE and TM apparent resistivities and phases. Let the kth ($k = 1, 2, 3, 4$) (real) observed response at site y_m ($m = 1, 2, \ldots, M$) and period T_n ($n = 1, 2, \ldots, N$) be denoted

by $O_k(y_m, T_n) \equiv O_{k,m,n}$ and let the corresponding theoretical response for a given model be $R_{k,m,n}$. Then the chi square misfit is defined as

$$\chi^2 = \sum_{k=1}^{K} \chi_k^2, \quad \chi_k^2 = \sum_{m=1}^{M} \sum_{n=1}^{N} \left(\frac{O_{k,m,n} - R_{k,m,n}}{\sigma_{k,m,n}} \right)^2$$

where $\sigma_{k,m,n}$ is the error (standard deviation) of the measurements, and $K \leq 4$ is the number of responses over which the misfit is measured. In our investigation we have always taken $K = 4$. Another measure of misfit is (Bevington, 1969, p. 187)

$$s^2 = \frac{1}{\nu} \sum_{k=1}^{K} \sum_{m=1}^{M} \sum_{n=1}^{N} w_{k,m,n} (O_{k,m,n} - R_{k,m,n})^2$$

where ν is the number of degrees of freedom and $w_{k,m,n}$ is the normalized weighting factor defined by

$$w_{k,m,n} = \frac{1/\sigma_{k,m,n}^2}{1/\bar{\sigma}_k^2}, \quad \frac{1}{\bar{\sigma}_k^2} = \frac{1}{MN} \sum_{m=1}^{M} \sum_{n=1}^{N} \frac{1}{\sigma_{k,m,n}^2}.$$

The number of degrees of freedom is $\nu = KMN - p$ where p is the number of model parameters available for adjustment in the minimization of the misfit. It will be noted that the two measures of misfit are related by the formula

$$s^2 = \frac{1}{\nu} \sum_{k=1}^{K} \bar{\sigma}_k^2 \chi_k^2.$$

Finally, the RMS misfit, preferred by many authors, is simply $\chi / \sqrt{KMN}$.

In this paper, the inversion method is applied to the MT data set obtained during the Kube Kabe project in Papua New Guinea (PNG) and provided by Chevron Niugini Ltd. of Australia. In the region surveyed, the surface geology reveals a series of anticlinal structures in outcropping Darai limestone representative of the verging Papuan Fold and Thrust Belt. It has been postulated that similar structures are present in the underlying sandstone reservoir, or Toro, and may have affected its formation and location. Specifically, it has been suggested that if the thrust has a shallow dip, a double Darai section will exist with no Toro in the core of the structure, but if the dip is sufficiently steep there will be no double section and the Toro will be present. One of the objectives of the inversion, then, is to map the thickness and dipping angle of the resistive Darai limestone in the survey region and to attempt to decide whether a double Darai section exists or not.

The response functions used in this investigation were $\frac{1}{2} \ln \rho^a$ and ϕ, where ρ^a is apparent resistivity and ϕ is the phase.

2. MT Data Processing

The data set consists of 10 sites along a profile aligned approximately N40E (Fig. 1) over a section of Darai Limestone below which conducting sediments are known to be present. At each site, MT responses at about 40 periods were derived in the period range covering 2.6×10^{-3} to 1.82×10^3 s. The data have been processed in four steps: (i) calculation of the strike direction and testing the dimensionality of the data; (ii) rotation of the MT tensor at each site into principal axes which lie along and perpendicular to the direction of strike; (iii) removal of local galvanic distortion or static shift; and (iv) search for the 'least-blocked' two-dimensional model compatible with both the E- and B-polarization observed data. Possible topographic effects have not been considered in the analysis.

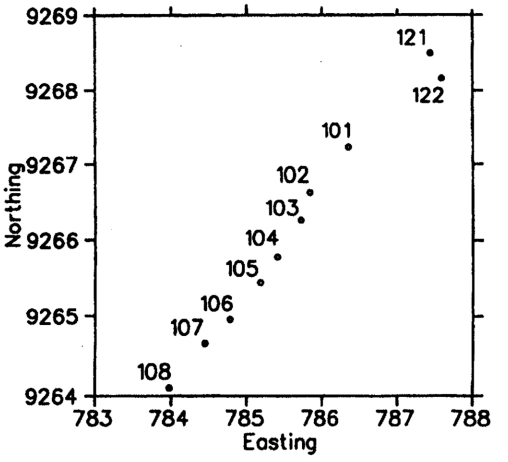

Fig. 1. The positions of the 10 PNG sites along a profile aligned roughly in the direction N40E.

The strike direction was calculated at each site by the procedure of Swift (1967; extracted in Vozoff, 1986), in which the axes are rotated until the off-diagonal elements of the MT impedance tensor are maximized. The resulting strike directions, shown in Fig. 2(a), vary within the range N45W to N90W as a function of period and site position. The average strike direction for the region was therefore taken to be approximately N60W. Jones and Groom (1993) have cautioned against this approach if the data are noisy or if there are 3D distortions present but the strike angle found is consistent with known geological structures in the region. Further evidence for this strike direction was provided by the GDS transfer functions, which permitted the calculation of induction ellipses at all sites except S22 and S21 (for which GDS transfer functions were unavailable). The major axes of the induction ellipses are aligned in the direction in which the vertical magnetic field is maximally correlated with the horizontal regional magnetic field (Banks, 1973) and are therefore perpendicular to the strike direction (although it should be mentioned that Jones and Groom (1993) again caution against the indiscriminate use of this method). The azimuths of the induction ellipses, shown in Fig. 2(b), display larger variations with period and site position than those in Fig. 2(a), but their *average* azimuthal direction is still approximately perpendicular to the 'Swift' direction of N60W and can be regarded as further confirmation that this is the correct angle of rotation to use. Scott and Jiracek (1994) obtained the same strike angle using a Groom-Bailey decomposition of the PNG data, which further validates our assumed strike angle.

The MT tensor was therefore rotated, at each period and at each site, into the principal axis system defined by the assumed strike direction of N60W and the direction N30E perpendicular to it, and the resulting E-polarization (or TE—'transverse electric') and B-polarization (or TM—'transverse magnetic') apparent resistivities and phases were calculated from the off-diagonal tensor components in the rotated frame. The corresponding maximum and minimum values of apparent resistivity and phase defining the error bars were obtained in similar manner by transforming the respective matrices of maximum and minimum values into the principal axis system. The MT data for both polarizations before and after rotation of the axes are presented in Fig. 3. The data labelled TE and TM in the unrotated coordinate system refer to the apparent resistivities and phases (ρ^a_{xy}, ϕ_{xy}) and (ρ^a_{yx}, ϕ_{yx}) respectively, where the x-axis points northwards and the y-axis eastwards.

To what extent the MT data can be represented by a two-dimensional model is judged by

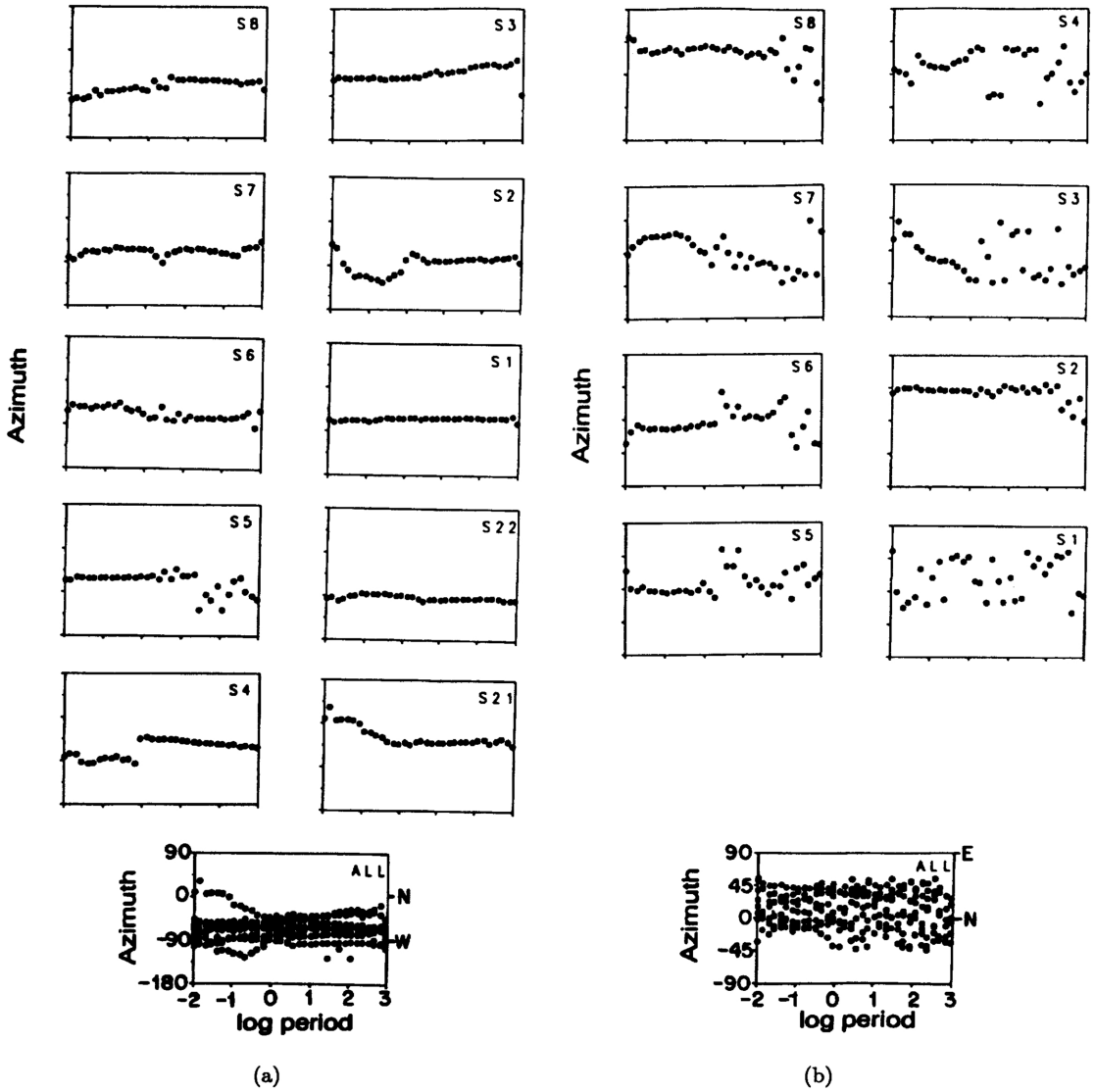

Fig. 2. (a) Plots of azimuth of strike direction (vertical scale in degrees) at each site against period (horizontal logarithmic scale) as given by the 'Swift rotation' of the coordinates. All strike directions are grouped together in the bottom diagram to show the average strike direction of N60W. (b) Similar to the plots in (a) but for the azimuth of the major axis of the induction ellipses. The values are calculated only at 8 sites for which GDS transfer functions were available.

computing 'two-dimensionality' parameters in the rotated frame of reference, such as skew and ellipticity of the impedance ellipses traced out in the complex plane by the elements of the MT tensor (Eggers, 1982). The calculated values of skew and ellipticity are shown in Figs. 4(a) and (b) respectively. The skew values are small at all sites, but the ellipticities display large variations with period and do not have any systematic trend from site to site, possibly indicating either strong local galvanic distortion (static shift) or that the assumption of two-dimensionality for

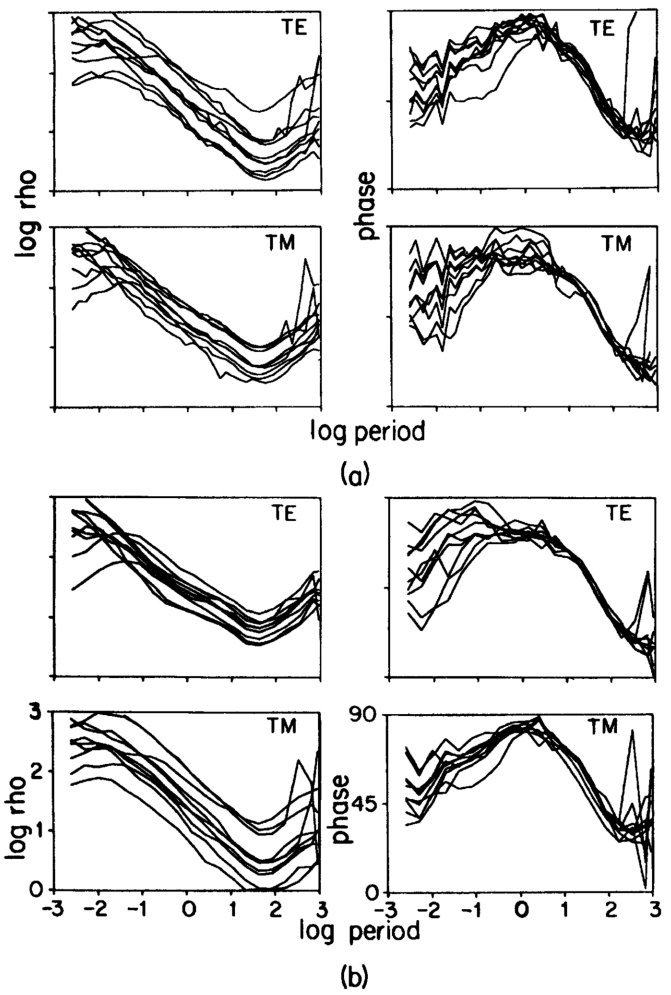

Fig. 3. TE and TM apparent resistivity and phase curves for all sites (a) before rotation of the coordinates, and (b) after rotation into the principal axis system.

the region is invalid. An examination of the assemblage of TE apparent resistivity curves for all sites (Fig. 3(b)), shows that they remain separated at longer periods which would imply that the structure at great depth is not one-dimensional. In contrast, pseudosections of the TE and TM phases, which are shown in Fig. 10 and which are not affected by static shift, do suggest one-dimensional structure at depth because only minimal lateral variations appear along the profile at long periods. It is concluded that a static shift must be present in the apparent resistivity curves. Note that the small contrasts seen in the pseudosections at the very long periods (>300 s) are attributed to noise in the data and are ignored. The pronounced lateral variations along the profile at short periods (<10 s) are quite evident in both the TE and TM pseudosections, and phase values greater than 50° indicate the presence of a conducting layer at shallow depth in the crust.

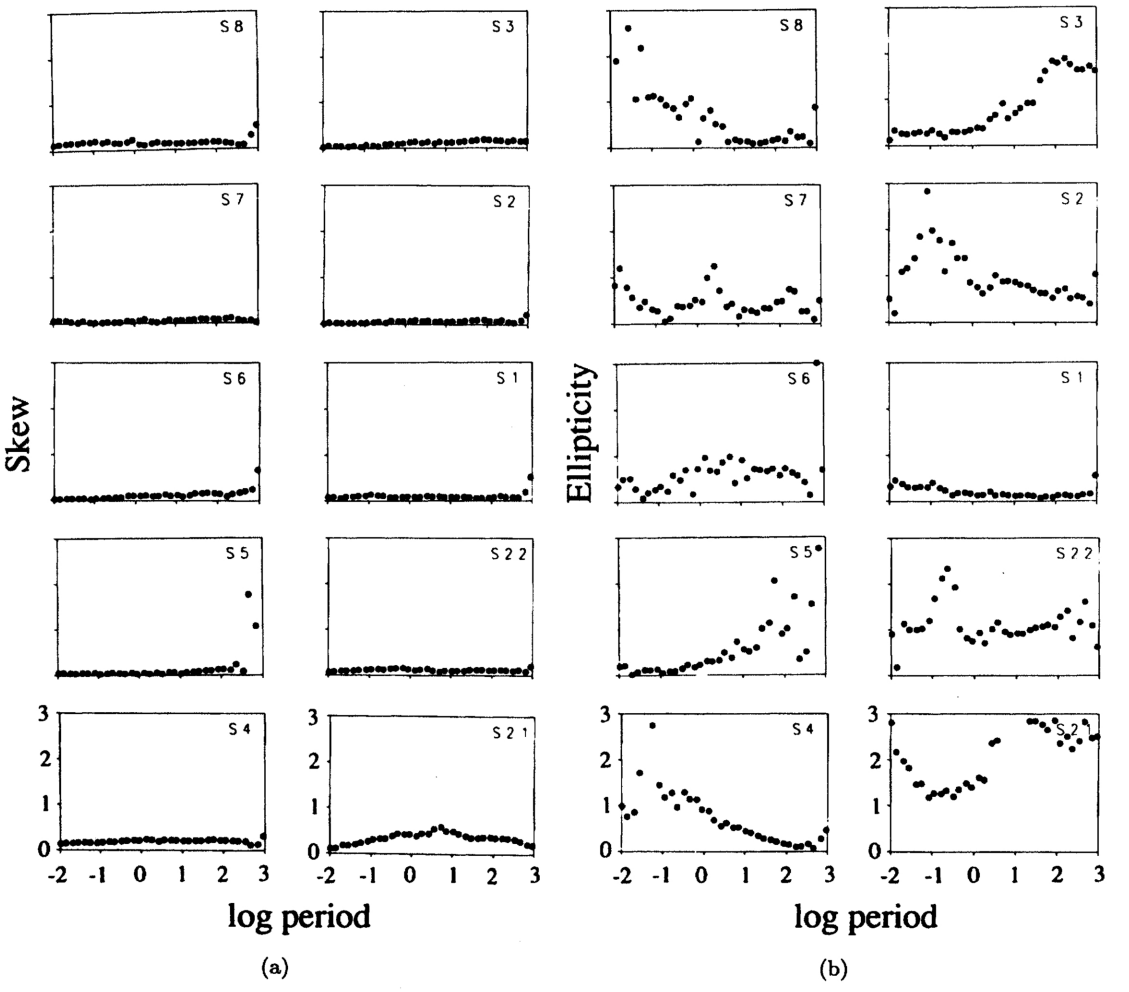

Fig. 4. Similar to Fig. 2 but showing the variation of (a) skew and (b) ellipticity of the impedance ellipses.

3. Static Shift Correction

Although a number of methods exist for correcting static shift (Jiracek, 1990), some of the more sophisticated ones, such as those devised by Bahr (1988) and Groom and Bailey (1989), can only be implemented with special computer programs which were not available to us. We have therefore preferred to take the simple approach suggested by Berdichevsky *et al.* (1989) and used recently by Marquis *et al.* (1995) in their analysis of the British Columbia data. Following this method we first displaced the TE apparent resistivity curves at all sites so that they assumed the value of 30 Ωm at the long period of 682.7 s, on the assumption that an approximate one-dimensional structure exists at great depths because the TE and TM phases approach each other at longer periods (Fig. 10). The 30 Ωm resistivity value was chosen as an approximate mean value at this period for all sites. The TM responses were then adjusted by matching them to the TE responses at the shortest period of 2.6×10^{-3} s, on the assumption that at sufficiently short periods the region probed appears uniform. A variation of this method in which the long-period data are allowed to follow a regional trend has been described and used by Jones *et al.* (1992)

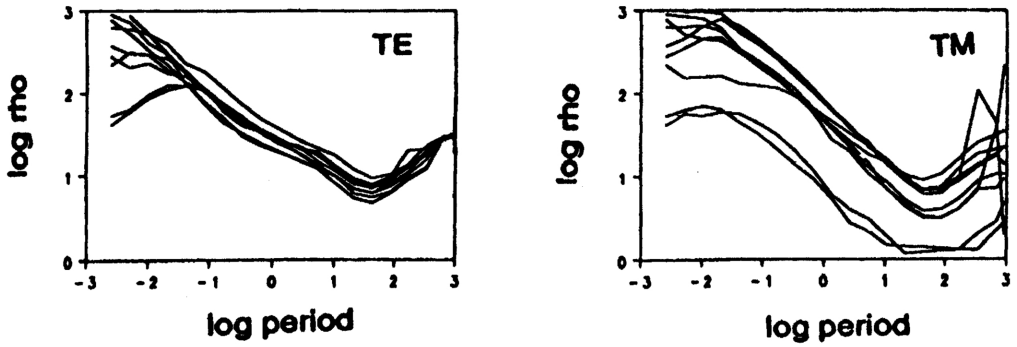

Fig. 5. TE and TM apparent resistivity curves corrected for static shift with respect to the principal (rotated) axes (cf. Fig. 3(b)).

and Jones and Dumas (1993). The corrected TE and TM apparent resistivity curves are shown in Fig. 5. The phase curves remain unaltered, of course. Our inversion scheme has been applied both to the raw MT data, and to the corrected data from which static shift has been removed.

4. Inversion of MT Data

The PNG anomaly was investigated by using all the 10 sites (S8, S7, S6, S5, S4, S3, S2, S1, S22, S21) whose locations with respect to the site S5 were taken as $y = -2.20, -1.48, -1.03, -0.40, 0, 0.58, 0.96, 1.73, 3.24, 3.41$ km. The relative distances were calculated using the easting and northing values supplied with the data.

For the minimizations alluded to below, both in the determination of the one-dimensional pseudosections and in the two-dimensional model optimization, we employ the same slow but robust routine used by Fischer and LeQuang (1981) and recently described by Schnegg (1993); Drs. Fischer and Schnegg have kindly made it available to us. It is based on a ravine search (Bevington, 1969, p. 207). An initial direction of decreasing s^2 (or χ^2) is first found by varying the parameters in the starting model and parameter space is then traversed in this direction until the value of s^2 (or χ^2) starts to increase. At this point, the directions orthogonal to the current path are explored, which may lead to a new direction of descent. If not, so that an increase in s^2 (χ^2) is detected in opposite directions along some line orthogonal to the current path, then the minimum value along that line is found by parabolic interpolation and the search is steered into a new direction defined by the location of this minimum. The search proceeds in this manner until the change in the misfit s^2 between successive trials is less than some prescribed percentage (0.01% in the present investigation), which indicates that a minimum value has been reached from which there is no escape, or until an upper limit on the number of calls to the routine has been exceeded. The latter usually means, in our experience, that the search has degenerated into unimportant meanderings around the minimum.

4.1 Models constructed from one-dimensional inversions of the PNG data

As an informative preliminary investigation, it is interesting to examine the TE and TM models constructed by juxtaposing the one-dimensional 'least-layered' structures at each site. They are generated by the automatic one-dimensional inversion scheme of Weaver and Agarwal (1993), which employs the same ravine search optimization procedure described above. Models have been compiled for both the raw (rotated) data and the data with static shift removed, and are displayed in Figs. 6(a) and (b). The presence of conductive sediments beneath the resistive

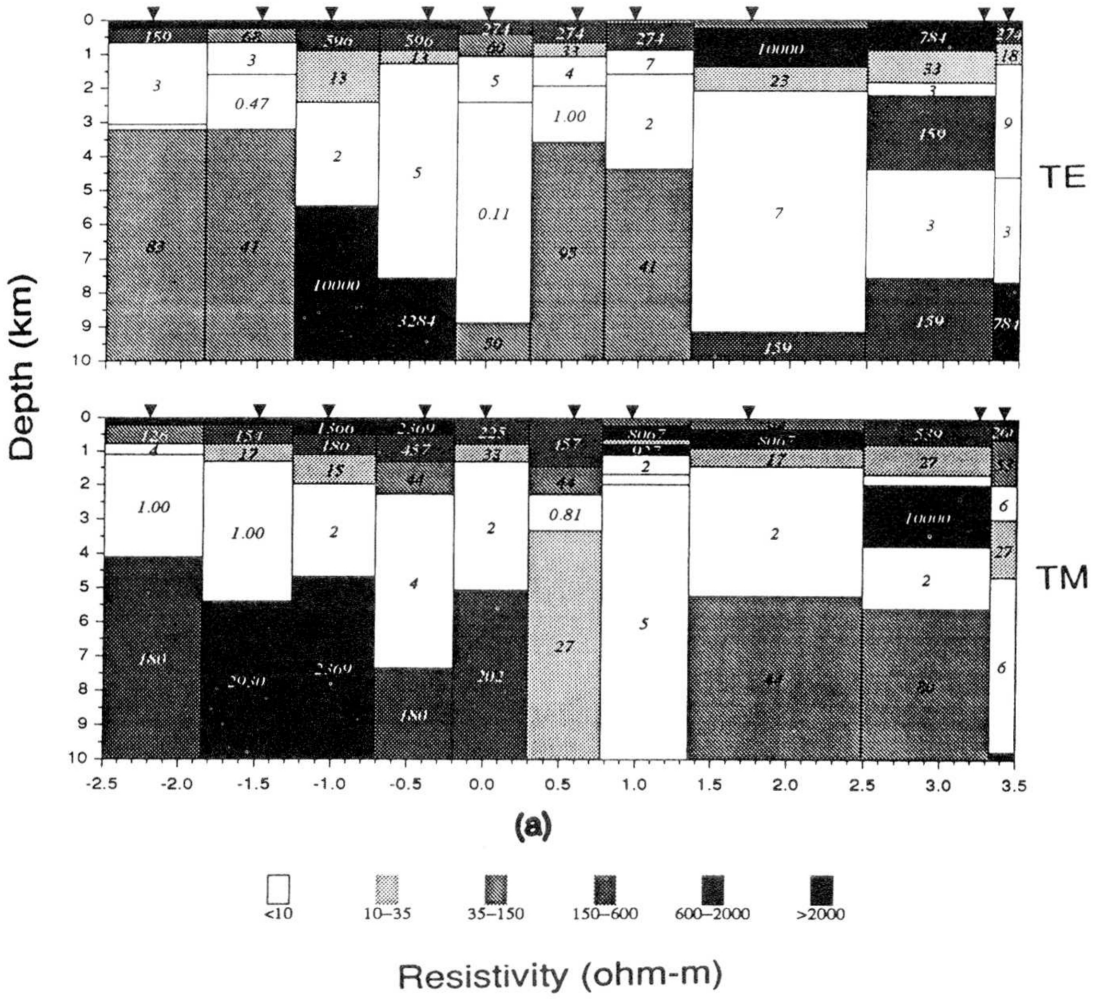

Fig. 6. TE and TM resistivity models formed by juxtaposition of the layered structures given by one-dimensional inversions at all sites for (a) the original PNG data as supplied but rotated into the principal axis system, and (b) the same data corrected for static shift. Resistivity values in Ωm are stated in the blocks; positions of the sites are marked by the inverted black triangles.

limestones at the surface is very apparent, but the more detailed characteristic features of the structure in the two models are rather different. The TE response suggests a resistive layer of increasing thickness along the profile from left (southwest) to right (northeast), whereas the TM response indicates a resistive layer that becomes thicker near the centre of the profile but shallower again towards its northeastern end. It is therefore preferable that both polarizations are considered when inverting the data. Hence, in the following subsection, we perform a joint inversion of the TE and TM data rather than inversions of each polarization separately.

4.2 Two-dimensional inversion of PNG data

The starting models with successively $3, 4, 5, \ldots$ columns are formed from an assemblage of one-dimensional 'least-layered' structures generated automatically from the TE data by the

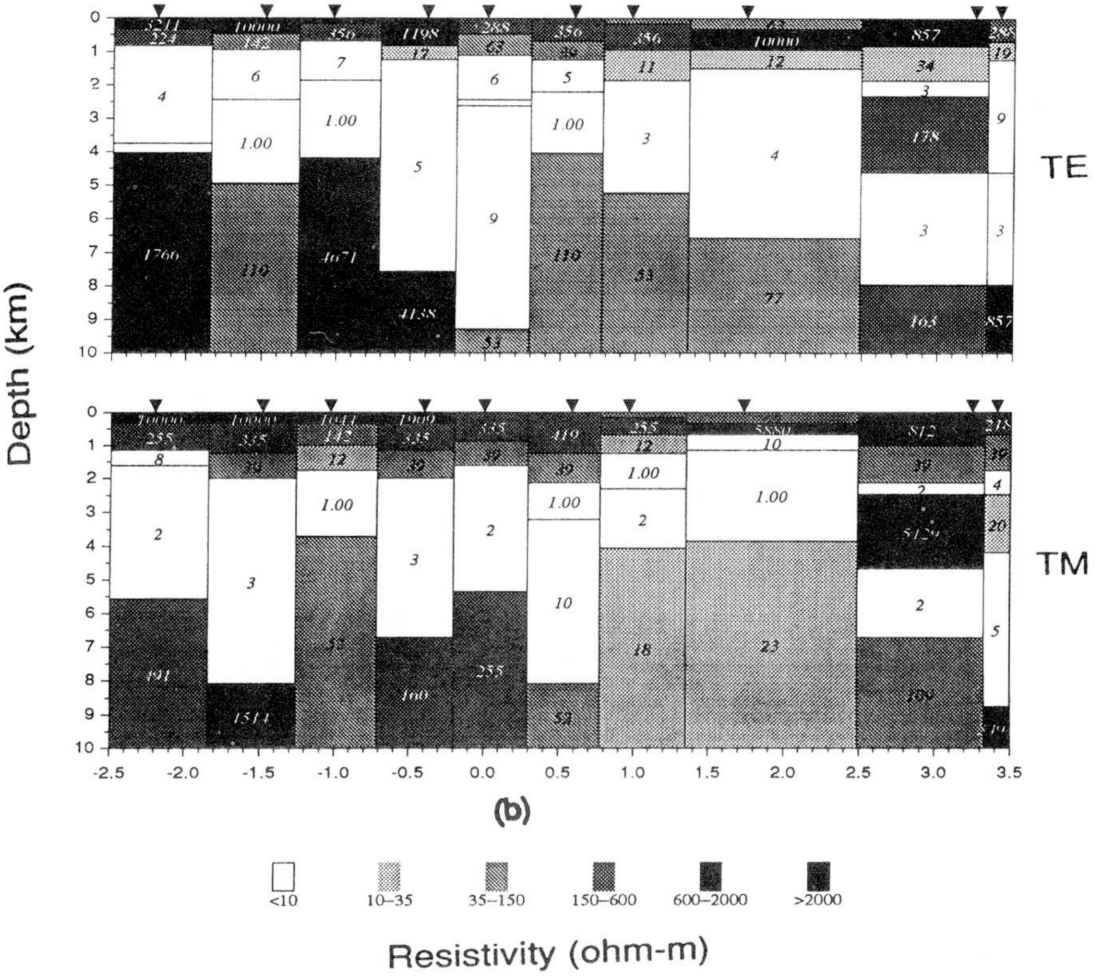

Fig. 6. (continued).

inversion program AUTOMOD (Weaver and Agarwal, 1993). Only the data for every other period of the 40 periods supplied were used for these one-dimensional inversions since they provided ample information for generating suitable starting models. Following the procedure outlined in our previous paper in which the COPROD2 data were inverted (Agarwal and Weaver, 1993), we first construct a 3 column starting model from one-dimensional inversions at 3 sites in the array profile, one in the centre, and two close to each end. The strategy adopted in making these selections is to favour, in the first instance, those sites with the greater number of layers, since they provide more flexibility in the optimization process. Vertical boundaries are inserted at the mid-points between the adjacent sites. The new site for the next starting model with 4 columns is chosen as the one where the one-dimensional inversion gives the greatest number of layers, whether on the left or right of the central site. The 5 column starting model is then formed by going to the site whose one-dimensional structure has the largest number of layers on the other side of the model, and so on, alternating back and forth from one side of the central site to the other. Further details on how the starting models are assembled have been described by Agarwal *et al.* (1993).

Since the resistivities, the horizontal boundaries, and also the positions of the vertical boundaries of the blocks, are free parameters for optimization in two dimensions, the method is highly demanding on computing time. Therefore, only 10 periods, $T = 0.0026$, 0.01, 0.042, 0.167, 0.667, 2.67, 10.67, 42.67, 170.70 and 682.70 s, were used for the two-dimensional inversion. It should be noted that the misfit was calculated for these 10 periods at all 10 sites during the optimization procedure, even though only a limited number of sites are used to define the starting models. The

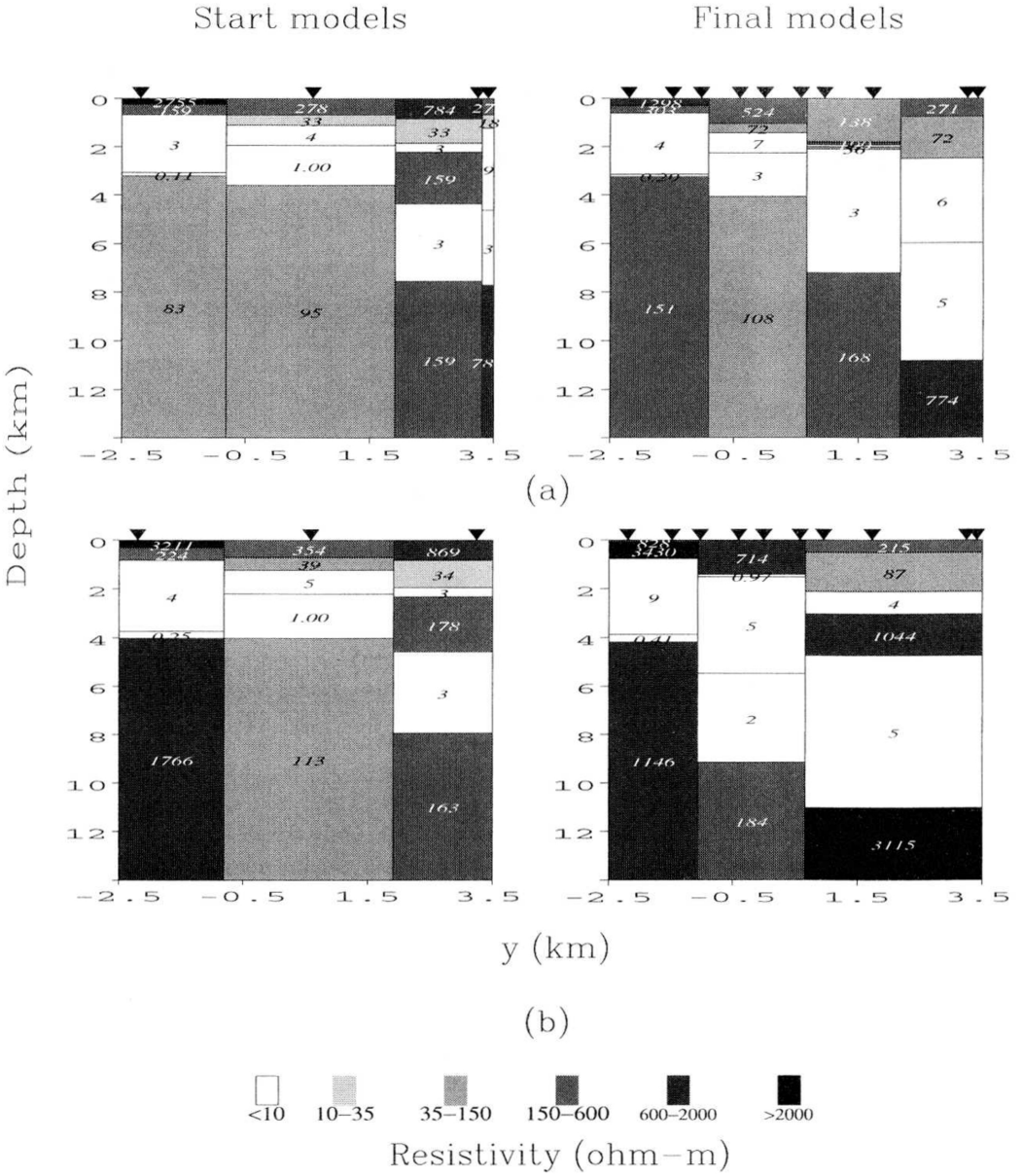

Fig. 7. Starting and final 'least-blocked' resistivity models obtained from (a) the original PNG data in the rotated coordinate system, and (b) the same data corrected for static shift.

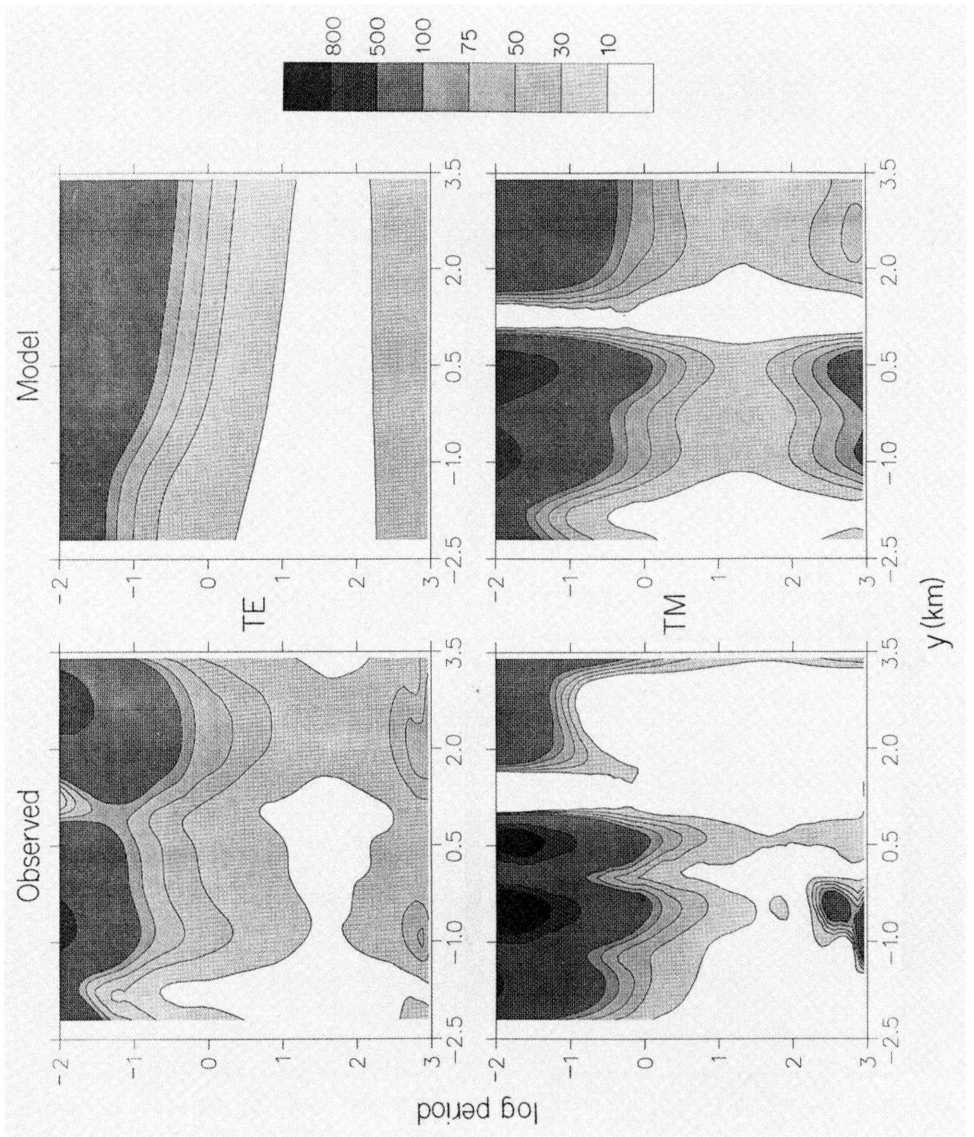

Fig. 8. Pseudosections of apparent resistivity responses (in Ωm) depicted for increasing periods (vertical log scale downwards) and different site positions (horizontal scale in km). The diagrams in the left- and right-hand columns respectively, are for the observed response and the calculated response of the model in Fig. 7(a). The upper two diagrams portray the TE responses, and the lower two the TM responses.

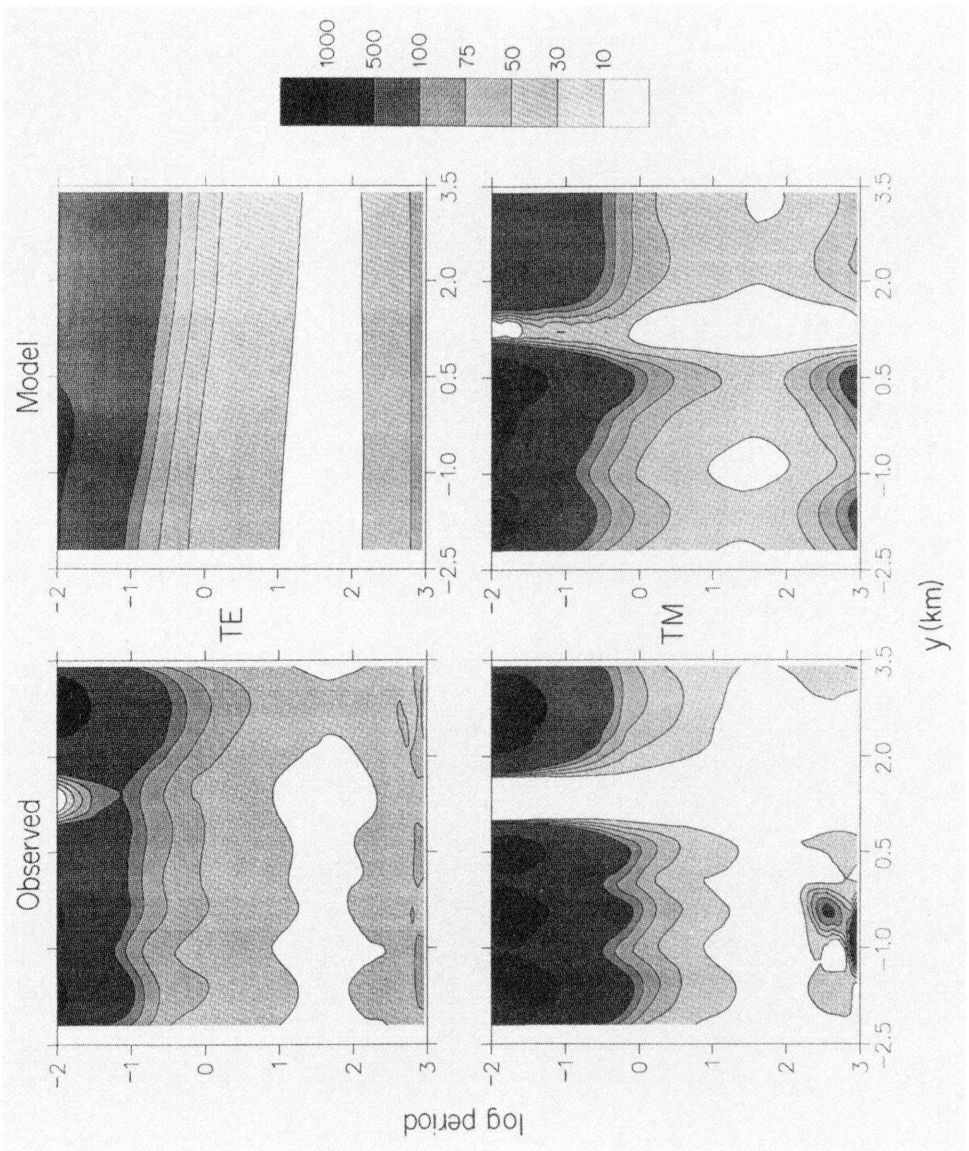

Fig. 9. As in Fig. 8 but for the dataset with static shift removed and with the calculated response for the model in Fig. 7(b).

procedure ceases when the addition of an extra column no longer gives a significant improvement in the fit between the model and observed responses.

The starting and final models for (a) the PNG data as supplied, and (b) the same data with static shift removed, are presented in Figs. 7(a) and (b) respectively. The misfit of the response of the final 4 column model in Fig. 7(a) is $s^2 = 7.57 \times 10^{-3}$ which translates into a RMS value of 8.9. It represented a significant improvement over the value for the preceding 3 column model. However, that was not the case when static shift was removed from the data; the final model in Fig. 7(b) has only 3 columns and a misfit of $s^2 = 5.75 \times 10^{-3}$ (corresponding to a RMS value of 6.6), which was not improved by proceeding to a 4 column model. Although these values are rather large, it should be noted that we have avoided the practice adopted by some authors of adjusting the error floors in order to reduce the RMS value nearer to 1.

The apparent resistivity responses of the models in Figs. 7(a) and (b) are compared in Fig. 8 with the uncorrected PNG data in the rotated coordinate system, and in Fig. 9 with the data corrected for static shift (Fig. 5). The comparisons are in the form of pseudosections with log period on the vertical scale (increasing downwards) and position y in km on the horizontal scale. The value of the response is depicted by the intensity of shading according to the relevant grey scale given. The observed phase responses depicted as pseudosections in Fig. 10 are unaffected, of course, by static shift, but the corresponding pseudosections in Fig. 11 of the phase responses of the models in Figs. 7(a) and (b) respectively, do differ slightly because the models themselves are different. It will be seen that the gross features of the observed apparent resistivity and phase responses are reproduced by both models, with the TM apparent resistivity responses being noticeably superior to the corresponding TE responses. The agreement of both the TE and TM phases at long periods is much better and reveals one-dimensional layering at depth (apart from some obvious noise in the observed data). The overall fit is not, however, particularly good. In efforts to improve the fit, we have tried inverting the TE and TM data separately and also performing a joint TE and TM inversion on the phase data alone. In each case, the fit of the responses used in the inversion was markedly improved but only at the expense of a severe deterioration in the fit of the other responses. It does not appear possible with our method to

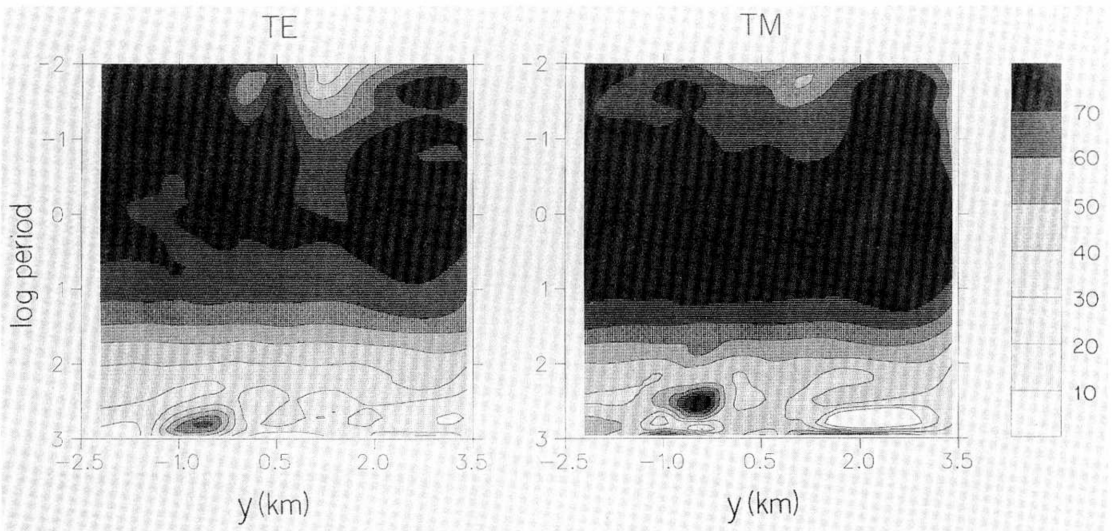

Fig. 10. Pseudosections constructed as in Fig. 8 except that only the observed phase responses (in degrees) are shown. The left- and right-hand diagrams depict the pseudosections for the TE and TM data respectively.

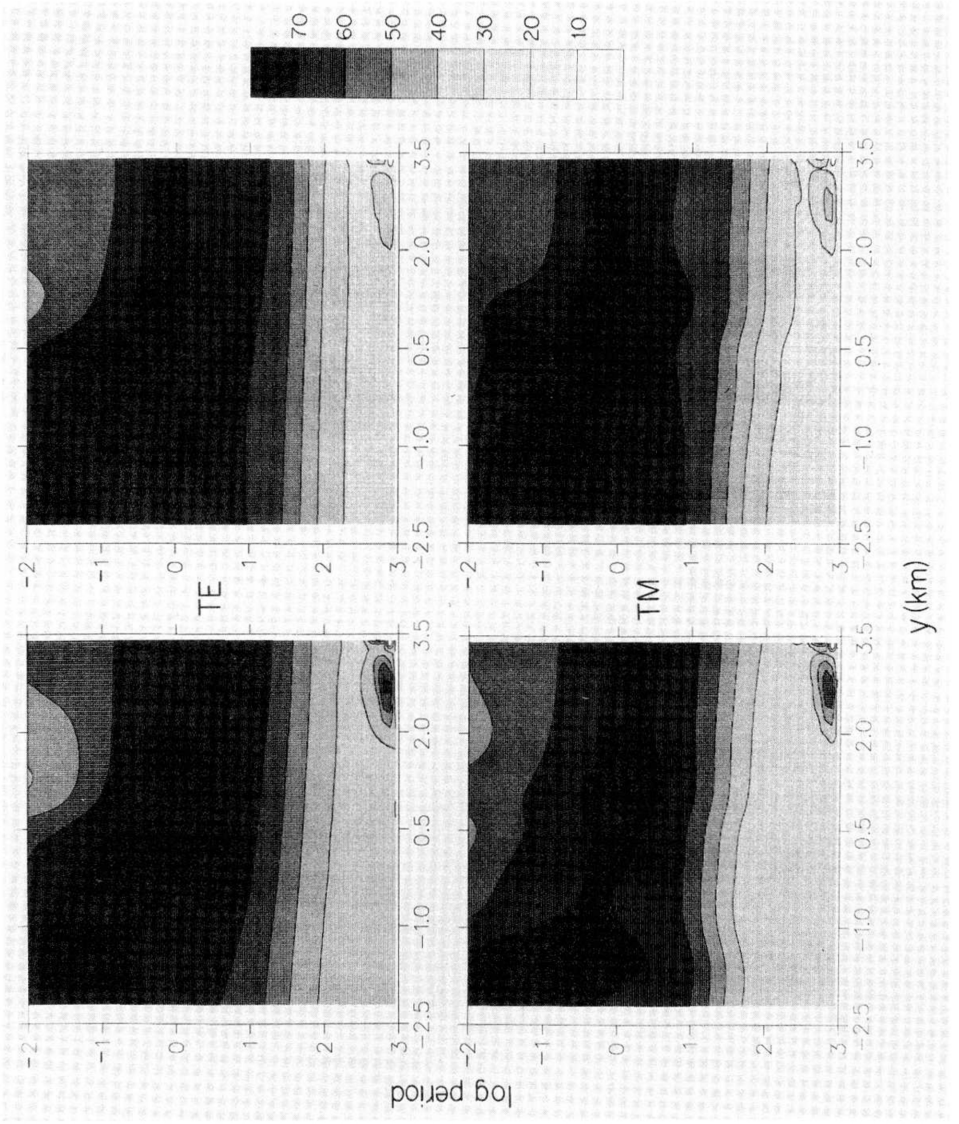

Fig. 11. Pseudosections of the calculated phase responses for the models in Fig. 7(a) (left-hand column) and Fig. 7(b) (right-hand column). The upper two diagrams portray the TE responses, and the lower two the TM responses.

obtain from the PNG dataset a two-dimensional model whose responses simultaneously fit all four observed responses to complete satisfaction. The discrepancies are possibly due to a combination of three-dimensional distortions and topographic effects.

The use of juxtaposed one-dimensional inversions as starting models (which, is the practice in other methods, such as AIM) may introduce some bias because the optimization procedure will probably be guided towards a local minimum of misfit close to the starting model which may not be the global minimum. In our method, some bias is also introduced in the sense that the final model cannot become more complex in structure than the starting model, only less so. If the misfit is unsatisfactory, however, more detail can be introduced into the structure by adding an extra column to the starting model and repeating the optimization. While this renders the method slower in execution than others, it does offer an alternative approach which is not subject to the smoothness constraint so prevalent in the various schemes involving over-parameterization.

As a test of possible bias and whether, in particular, the resistive layer sandwiched between two conductive blocks on the right of the final model in Fig. 7(b) is meaningful or not, a numerical experiment was conducted in which the resistivity of this layer was set at 10 Ωm instead of 1044 Ωm. This was equivalent to removing the resistive layer since the blocks above and below it have resistivities of the same order of magnitude, 4 Ωm and 5 Ωm respectively. It was interesting to discover that optimizing this new starting model seriously affected only the parameters defining the layer in question; its thickness was increased slightly and its resistivity was magnified fivefold. Thus, the new final model closely resembled the one shown in Fig. 7(b) (all the other parameters changed only negligibly). This result suggests that even though sandwiched resistive layers are notoriously difficult to image in magnetotellurics, the layer appearing in our final model Fig. 7(b) is indeed a feature that is required by the dataset which has been corrected for static shift.

5. Conclusions

For both sets of data, the final models are fairly simple when compared with the juxtaposition of one-dimensional inversions shown in Figs. 6(a) and (b). The layer of resistive limestone and the underlying conductive sediments are clearly visible in both final models, which closely resemble each other except for the presence of an extra conductive layer on the right of the 3 column model in Fig. 7(b), i.e. towards the northeastern end of the profile. The thickness of the resistive limestone increases from a range of 0.6–0.8 km in the southwest to about 2.1–2.4 km in the northeast. The depth to the top of the resistive basement also varies along the profile, from about 4 km on the southwestern side to about 11 km in the northeast. This depth may not be properly resolved, however, because of large error bars occurring in the data at the longer periods. Although not shown here, we also carried out the inversion using equal weights of unit magnitude for calculating the misfit value (which corresponds to assuming that the data are error free). The resistive basement in the final models was located at a fairly uniform depth of about 6–7 km along the whole profile in this case, which suggests that the depth of basement is very sensitive in our inversion scheme to the error bars provided with the data.

Although the general trends of the apparent resistivity and phase responses of the final models in Figs. 7(a) and (b) match the corresponding observed responses quite well for both TE and TM polarizations, the individual fit at each period and site is not as good as we have found with other data sets—e.g. with COPROD2. This less than satisfactory outcome could be attributed to a possible underestimation of the error bars in the PNG data, the neglect of topographic effects, or perhaps the assumption of two-dimensionality which might be invalid for this particular region. Whatever the reason, it is still interesting to note that both the one-dimensional 'least-layered' and the two-dimensional 'least-blocked' inversions of the PNG data give models which consistently reveal a layer of conductive sediments between the Darai limestones at the surface and a resistive basement, and that the possibility of a split conductive layer at the northeastern end of the profile

is suggested by the data that has been corrected for static shift.

The authors are indebted to Dr. S. C. Constable and an anonymous referee for their constructive comments which led to a great improvement in the final version of this paper. Data from the Kube Kabe project in the region of Papua New Guinea (PNG) were kindly made available by Chevron Niugini Ltd., Australia and distributed by Dr. Alan Jones. Dr. Guy Marquis is thanked for helpful discussions on static shift removal. Support from the Natural Sciences and Engineering Research Council of Canada and the University of Victoria is gratefully acknowledged.

REFERENCES

Agarwal, A. K. and J. T. Weaver, Inversion of the COPROD2 Data by a method of modelling, *J. Geomag. Geoelectr.*, **45**, 969–983, 1993.

Agarwal, A. K., Helena E. Poll, and J. T. Weaver, One- and two-dimensional inversion of magnetotelluric data in continental regions, *Phys. Earth Planet. Int.*, **81**, 155–176, 1993.

Bahr, K., Interpretation of the magnetotelluric impedance tensor: regional induction and local telluric distortion, *J. Geophys.*, **62**, 119–127, 1988.

Banks, R. J., Data processing and interpretation in geomagnetic deep sounding, *Phys. Earth Planet. Int.*, **7**, 339–348, 1973.

Berdichevsky, M. N., L. L. Vanyan, and V. I. Dmitriev, Methods used in the USSR to reduce near-surface inhomogeneity effects on deep magnetotelluric sounding, *Phys. Earth Planet. Int.*, **53**, 194–206, 1989.

Bevington, P. R., *Data Reduction and Error Analysis for the Physical Sciences*, McGraw-Hill, New York, 1969.

deGroot-Hedlin, C. D. and S. C. Constable, Occam's inversion to generate smooth, two-dimensional models from magnetotelluric data, *Geophysics*, **55**, 1613–1624, 1990.

Eggers, D. E., An eigenstate formulation of the magnetotelluric impedance tensor, *Geophysics*, **47**, 1204–1214, 1982.

Fischer, G. and B. V. LeQuang, Topography and minimization of the standard deviation in one-dimensional magnetotelluric modelling, *Geophys. J. R. astr. Soc.*, **67**, 279–292, 1981.

Groom, R. W. and R. C. Bailey, Decomposition of magnetotelluric impedance tensors in the presence of local three-dimensional galvanic distortion, *J. Geophys. Res.*, **94**, 1913–1925, 1989.

Jiracek, G. R., Near-surface and topographic distortions in electromagnetic induction, *Geophys. Surv.*, **11**, 163–203, 1990.

Jones, A. G., The COPROD2 dataset: tectonic setting, recorded MT data, and comparison of models, *J. Geomag. Geoelectr.*, **45**, 933–955, 1993.

Jones, A. G. and I. Dumas, Electromagnetic images of a volcanic zone, *Tectonophys.*, **81**, 289–314, 1993.

Jones, A. G. and R. W. Groom, Strike-angle determination from the magnetotelluric impedance tensor in the presence of noise and local distortion: rotate at your peril!, *Geophys. J. Int.*, **113**, 524–534, 1993.

Jones, A. G., D. I. Gough, R. D. Kurtz, J. M. DeLaurier, D. E. Boerner, J. A. Craven, R. G. Ellis, and G. W. McNeice, Electromagnetic images of regional structure in the southern Cordillera, *Geophys. Res. Lett.*, **12**, 2373–2376, 1992.

Marquis, G., A. G. Jones, and R. D. Hyndman, Coincident conductive and reflective middle and lower crust in southern British Columbia, *Geophys. J. Int.*, **120**, 111–131, 1995.

Oldenburg, D. W. and R. G. Ellis, Inversion of geophysical data using an approximate inverse mapping, *Geophys. J. Int.*, **105**, 325–353, 1991.

Schnegg, P.-A., An automatic scheme for 2-D magnetotelluric modelling, based on low-order polynomial fitting, *J. Geomag. Geoelectr.*, **45**, 1039–1043, 1993.

Scott, C. and G. R. Jiracek, Two-dimensional distortion correction, topographic analysis, and modeling of PNG data (extended abstract), *2nd International MT Data Interpretation Workshop*, Cambridge, Aug. 4–7, 1994.

Smith, J. T. and J. R. Booker, Rapid inversion of two- and three-dimensional magnetotelluric data, *J. Geophys. Res.*, **96**, 3905–3922, 1991.

Swift, C. M., Magnetotelluric investigation of an electrical conductivity anomaly in the southwestern United States, Ph.D. thesis, Dept. Geol. Geophys., M.I.T., Camb., MA, 1967.

Vozoff, K., (ed.), *Magnetotelluric Methods*, Soc. Expl. Geophys. Reprint Ser. No. 5, Publ. by Soc. Expl. Geophys., Tulsa, OK, ISBN 0-931830-36-2, 1986.

Weaver, J. T. and A. K. Agarwal, Automatic one-dimensional inversion of magnetotelluric data by the method of modelling, *Geophys. J. Int.*, **112**, 115–123, 1993.